Original Article

Development of Highly Reliable Power and Communication System for Essential Instruments Under Severe Accidents in NPP

CrossMark

Bo Hwan Choi [a], Gi Chan Jang [a], Sung Min Shin [a], Soo Ill Lee [b], Hyun Gook Kang [a], and Chun Taek Rim [a,]*

[a] *Department of Nuclear and Quantum Engineering, Korea Advanced Institute of Science and Technology, 291 Daehak-ro, Yuseong-gu, Daejeon, 34141, South Korea*
[b] *I&C Group, Korea Hydro & Nuclear Power Co., Ltd, Central Research Institute, 70 Yuseong-daero, Yuseong-gu, Daejeon, 34101, South Korea*

ABSTRACT

This article proposes a highly reliable power and communication system that guarantees the protection of essential instruments in a nuclear power plant under a severe accident. Both power and communication lines are established with not only conventional wired channels, but also the proposed wireless channels for emergency reserve. An inductive power transfer system is selected due to its robust power transfer characteristics under high temperature, high pressure, and highly humid environments with a large amount of scattered debris after a severe accident. A thermal insulation box and a glass-fiber rein-forced plastic box are proposed to protect the essential instruments, including vulnerable electronic circuits, from extremely high temperatures of up to 627°C and pressure of up to 5 bar. The proposed wireless power and communication system is experimentally verified by an inductive power transfer system prototype having a dipole coil structure and pro-totype Zigbee modules over a 7-m distance, where both the thermal insulation box and the glass-fiber reinforced plastic box are fabricated and tested using a high-temperature chamber. Moreover, an experiment on the effects of a high radiation environment on various electronic devices is conducted based on the radiation test having a maximum accumulated dose of 27 Mrad.

1. Introduction

The availability of emergency countermeasures after a severe accident is the most critical issue in nuclear power plant (NPP) safety [1—8]. Since the Fukushima accident, reliable and continuous measurements of the NPP during a severe accident are critical to support decision-making that is adaptable to rapidly varying accident environments. From several previous

severe accidents, it was found that the loss of measurements is the major cause of delays in crucial decisions such as a seawater injection or public evacuation, and these delays consequently lead to uncontrollable public fears of NPPs.

A sequence of measurement loss after a severe accident can be determined as follows:

1. A beyond design basis accident involving significant core degradations occurs [1]
2. Major instruments and power/communication lines are exposed to extremely high temperature, pressure, and moisture, which are mainly due to both reactor failures and poor accident management
3. The instruments and connected cables are damaged and permanent instrument failure happens when repairs to the instruments are not available due to the high radiation environment of a severe accident [3,4].

To overcome the physical failure of currently installed instruments and cables, which are designed by following the equipment qualification based on design-based accidents, several methodological approaches for enhancing the reliability of equipment have been researched [5−8]. The previous methodologies can be classified into the following three categories, where a configuration of the collective results is depicted in Fig. 1:

1. Problem definition: intensified temperature and pressure profiles were suggested for reviewing and/or designing the protection of the NPP equipment against severe accident environments.
2. Increase in redundancy: additional instrument channels were applied as extra redundancies to deal with the malfunctions and degradations of the existing channels.
3. Physical reinforcement: instead of replacing all damageable equipment, physical protective remedies against extreme temperature and pressure conditions were introduced for existing instruments and cables.

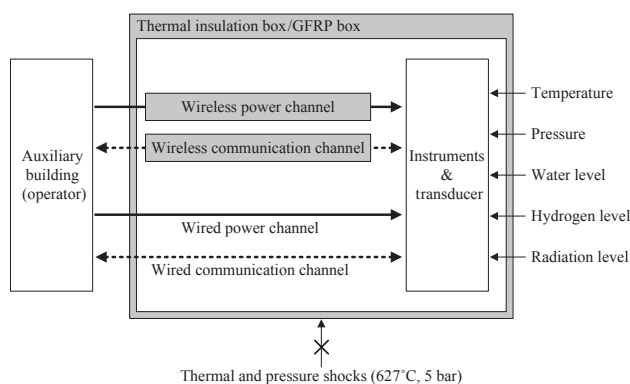To identify the design requirements of Categories 2 and 3, the peak temperature and pressure during a severe accident can be determined by various methods [8,9]. As shown in Fig. 2, a temperature profile during the 72 hours after an accident having a peak temperature of 627°C and a long-term ambient temperature of 187°C was evaluated based on simulations of various points in the containment building. In spite of that, lower temperature profiles can be expected in some regions, such as the upper parts of the containment building. The highest peak temperature of 627°C is selected as a design requirement in this paper to achieve a conservative design. A hydrogen explosion can be considered as the worst condition that puts maximum stress on the equipment. From equivalent experiments by the Electric Power Research Institute [10], the peak pressure value can be determined as 5 bar (or 72.5 psig).

To deal with the loss of conventional wired power and communication cables, reserved wireless channels have been suggested for both the power channel and the communication channels by adopting an inductive power transfer system (IPTS) and radio frequency (RF) communication, respectively [7,8,11,12].

Direct use of the temperature and pressure conditions in Category 1 as design requirements of the NPP equipment is impractical due to the extremely high cost. Therefore, a thermal insulation box and a glass-fiber reinforced plastic (GFRP) box were conceptually proposed to protect only some of the equipment, which is essential for evaluating the NPP integrity, from extremely high temperature and pressure [7,8].

In this paper, the design principles of "increasing redundancy" and "physical reinforcement" are proposed and experimentally verified with relevant prototypes. As the wireless power channel, 10-W level IPTS using a dipole coil resonance system is designed over a 7-m distance, where the target distance matches the length of the main route of the conventional power/communication cables from the inner wall to the outer wall of the containment building shown in Fig. 1. The wireless communication channel is composed of two Zigbee modules covering a 10−20 m range without any

Fig. 1 − Configuration of the proposed highly reliable power and communication system for essential measurements in the nuclear power plant. GFRP, glass-fiber reinforced plastic.
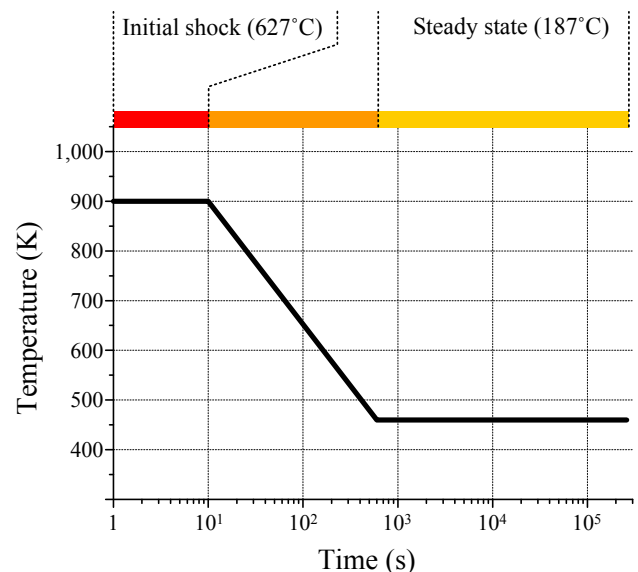

Fig. 2 − Dynamic temperature profile of the containment building during a severe accident lasting 72 hours.

data loss for 72 hours. The design of the proposed thermal insulation box consisting of a water layer and a microporous insulator is provided based on a simplified model in Yoo et al. [13] to isolate the equipment from the heat shock. A GFRP box, having a thickness of 10 mm, was designed to protect the proposed IPTS coils from the heat and pressure. Both the insulation box and the GFRP box were experimentally verified using a fabricated high-temperature chamber that can mimic the temperature profile in Fig. 2.

The rest of this paper is organized as follows: Section 2 presents design principles for the proposed highly reliable power and communication system consisting of the wireless power/communication channels, the thermal insulation box, and the GFRP box; Section 3 shows experimental verifications of the performance of the proposed redundant wireless channels and the physical protection boxes with consideration of high temperature and radiative environments. Conclusions are provided in Section 4.

2.   Design of the proposed highly reliable power and communication system

In this section, the proposed highly reliable power and communication system is categorized into four subsystems, namely the 10-W level wireless power channel, RF wireless communication channel, thermal insulation box, and GFRP box. Both the wireless power and communication channels are applied with currently installed wired channels to increase reliability. Both the thermal insulation box and the GFRP box work with any NPP equipment that is likely to be exposed to extreme temperature and pressure. In the following subsections, the design requirements of each subsystem are thoroughly investigated and fulfilled by prototype design, where the design requirements of each subsystem are identified in Table 1.

2.1.   10-W level wireless power channel

As shown in Fig. 3, a target distance of 7 m was selected for a wireless power transfer to power sensors and transducers in NPP, considering typical routes of the power cables from an inner wall to an outer wall of the containment building. Due to the extreme environments, which vary dynamically during a severe accident, most of the wireless power transfer methods in NPPs are highly restricted, as tabulated in Table 2. As a result of comparative evaluation on the robust powering characteristic, the IPTS method having a dipole coil at each transmitting (Tx) and receiving (Rx) side is selected. The output power of the proposed ITPS is set as 10 W according to the load estimation in Yoo et al. [8], which can cover typical power consumptions of two wireless sensor sets, where a wireless sensor set consists of a microprocessor, an RF communication module, and an instrument including its transducer. A typical pressure transmitter (Rosemount 1154), which consumes approximately 1 W for its normal operation, is selected in this paper for the load power estimation of the proposed IPTS.

The Curie temperature of typical Mn−Zn ferrite cores, which compose the dipole coils, is approximately 300°C, and the typical operating temperature of the cable is also limited to as low as 200°C, assuming that a Teflon coated cable is used. Moreover, the ferrite core is fragile and susceptible to corrosion. Therefore, additional physical reinforcement is required considering vulnerable coil characteristics in extreme environments.

As shown in Fig. 4, an electromagnetic interference issue is reviewed using finite element method simulations, where the proposed 10-W level IPTS is designed as follows [11]: an aluminum shielding box is introduced to satisfy the magnetic field emission restriction in the containment building, which is depicted in Fig. 5; the magnetic field density inside a 1-mm thick aluminum box satisfies the magnetic field emission restriction required by the Nuclear Regulatory Commission of 105 BpT (178nT) at 20 kHz [14]. Note that the proposed wireless

| Table 1 − Summarized design requirements of each subsystem.			
Increase in redundancy with wireless channels		**Physical reinforcement**	
IPTS	RF communication	Thermal insulation box	GFRP box
• 10-W powering over 7 m for two wireless sensor sets • Limited dipole length of 2 m • No EMI issue with other equipment used together • Operating with ferrite cores having a low Curie temperature of ~300°C • Operating with high-frequency applicable wire having a low insulator melting temperature of ~200°C • Requiring additional physical reinforcements under the given ambient temperature and pressure (187−627°C, 5 bar)	• Data transfer over 7 m • No cross interference with the IPTS • No error or data loss for 72 hr • Satisfying low operating temperature of Zigbee modules/microprocessors (~85°C) • Requiring additional physical reinforcements under the given ambient temperature and pressure (187−627°C, 5 bar)	• Keeping the cavity temperature lower than 85°C for 72 hr with the given temperature outside of the cavity (187−627°C) • Imperfect thermally isolated system due to conductive incoming cables from the outside into the cavity • Maintaining structural integrity for the given ambient temperature and pressure (187−627°C, 5 bar)	• Maintaining structural integrity for the given ambient temperature and pressure (187−627°C, 5 bar) • No disturbance to the magnetic field or electric field for use together with IPTS and RF communication
EMI, electromagnetic interference; IPTS, inductive power transfer system; GFRP, glass-fiber reinforced plastic; RF, radio frequency.			
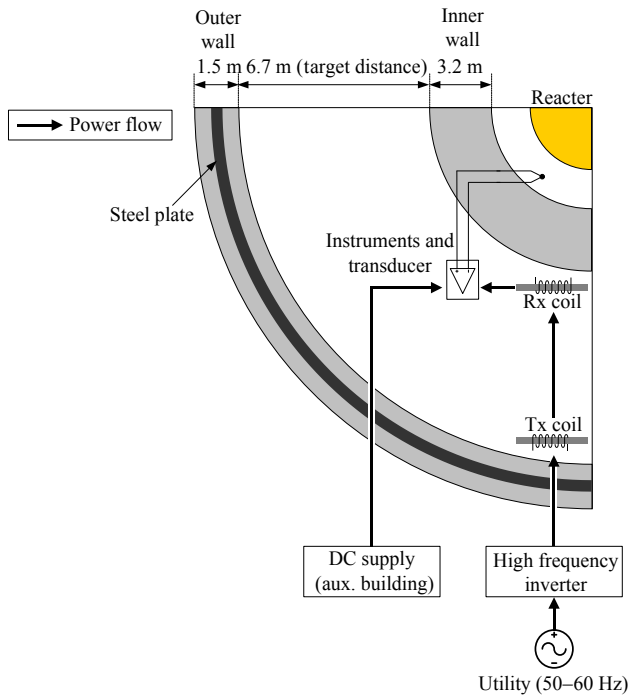
Fig. 3 − **Configuration of the proposed wireless power channel installed in the containment building with the conventional wired channel from the auxiliary building, where a quarter of the containment building is illustrated. aux, auxiliary; DC, direct current; Rx, receiving side; Tx, transmitting side.**

Fig. 4 − **Inductive power transfer system simulation result with an aluminum shielding box at the operating frequency of 20 kHz when I_{tx} = 40A and 30 turns for each coil. Rx, receiving side; Tx, transmitting side.**

channel operates only for the loss of wired channels during a severe accident; hence, there is no issue of electromagnetic interference with the currently installed equipment, which would no longer be available during a severe accident.

2.2. RF wireless communication channel

The design of the proposed wireless communication channel is quite similar to the wireless power channel design. Considering the required communication distance of 7 m,
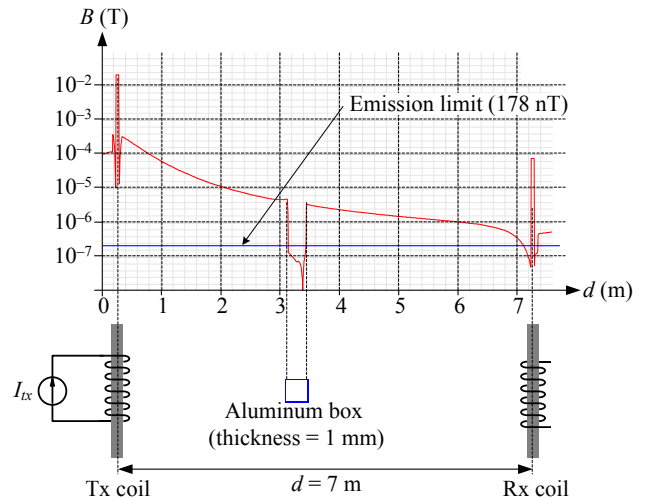
which is the same as the required wireless power transfer distance, RF communication is selected, where the magnetic field communication technique is not preferred due to the technical immatureness and the cross interference with IPTS. Among the available RF communication candidates, Zigbee is selected after considering its low power consumption and relatively good data transfer ability.

Just as with the vulnerability issues in the previous section, applicable Zigbee modules and auxiliary electronic circuits have a maximum operating temperature between 85°C and 120°C, which is mainly due to the performance of state-of-the-art semiconductor devices inside the module. Hence, an additional reinforcement should be installed together with the proposed wireless communication channel to endure the extreme ambient conditions.

Fig. 6 shows a block diagram of the proposed wireless communication channel, which can substitute for a conventional current transducer converting a voltage signal to a current signal ranging from 4 mA to 20 mA. Commercial

| Table 2 − Comparison among possible wireless power channels.			
Methods	Advantages	Disadvantages	Remarks
RF	• Relatively good in environment containing steam, vapor, and/or debris (as compared with the laser type)	• Impossible to penetrate water layers and/or metal objects • High EMF/EMI	Unacceptable
Laser	• No EMI/EMF due to the highest straightness	• Impossible to penetrate obstacles • Difficult to overcome environments containing steam, vapor, and/or debris	Unacceptable
CMRS	• Relatively good for long-distance wireless power transfers (due to the high quality factor)	• Large diameter of coils • Complex structure • Hypersensitive performance	Unacceptable
IPTS	• Simple structure • High output power • Long-distance power transfer with a low quality factor	• High EMF/EMI • An EMI/EMF shield can be achieved by using a metal plate	Acceptable
CMRS, coupled magnetic resonance system; EMF, electromagnetic fields; EMI, electromagnetic interference; IPTS, inductive power transfer system; RF, radiofrequency.			
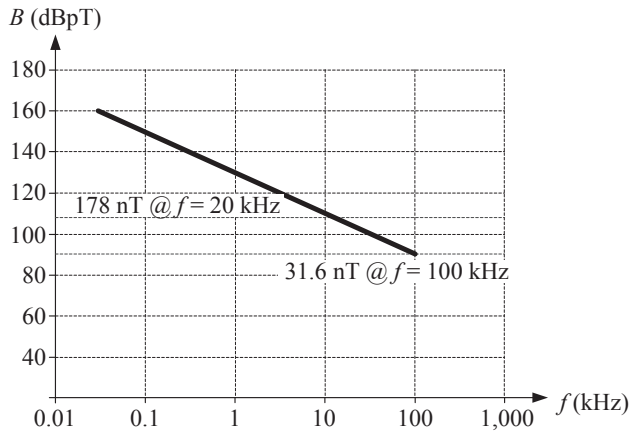
Fig. 5 – Magnetic field emission restriction from the Nuclear Regulatory Commission, RE101: 178 nT and 31.6 nT at the operating frequencies of 20 kHz and 100 kHz, respectively [14].

Zigbee modules are used with microprocessors, which convert analog input to digital output, and single or cascaded noise filters can be used together depending on the input noise level. The 5-W level wireless sensor set is represented as gray-colored blocks in Fig. 6, where it can be powered by both the wired and wireless power channels. Considering both power channels are alternating current sources, a diode rectifier and a battery are used together with the wireless sensor set to guarantee the stable direct current supply voltage, where sudden voltage fluctuations can be critical to the quality of the wireless communication.

2.3. Thermal insulation box

As identified from the temperature profile in Fig. 2, the initial thermal shock of 627°C and a relatively high long-term ambient temperature of 187°C are critical to the NPP equipment. The main roles of the proposed thermal insulation box

are protecting the selective equipment from the thermal shock and providing operable temperature to the equipment.

The design of the proposed thermal insulation box is conducted based on the simplified heat transfer model in Yoo et al. [13] and finite element method simulation. As shown in Fig. 7A, the thermal insulation box consists of two layers with high thermal coefficients. The external layer is a microporous insulator, which is Super-G from Microtherm in this paper, having a thickness of 75 mm. The inner water layer of various thicknesses in a range of 100 mm to 300 mm, also delays heat transfer from ambient to the cavity, which is prepared for the equipment installation. As shown in Fig. 7B, the cavity temperature does not exceed 80°C for 72 hours of simulation, where the ambient condition follows the temperature profile in Fig. 2.

Stainless steel is used to build the frame of the thermal insulation box considering its robustness against high temperature and excess moisture.

2.4. GFRP box

The GFRP box is designed to provide the equipment with a protective case from high pressure including the mechanical shock of scattered objects due to a hydrogen explosion or severe vibration caused by natural disasters. The material of GFRP was selected after considering that GFRP has no degrading effect on the proposed wireless power and communication channels. Fig. 8A shows a design example of the proposed GFRP box for the 2-m long dipole coil used in the proposed wireless power channel. Satisfying both design Eqs. (1) and (2) [8], a thickness of 10 mm was selected for the proposed GFRP box to achieve both structural integrity against pressure shock of 5 bar and heat transfer delay against the initial heat shock of 627°C.

Figs. 8B and 8C show cross sectional diagrams of the proposed GFRP box with the dipole coil inside. The heat transfer from the ambient to the dipole coil inside the GFRP box can be determined as follows:
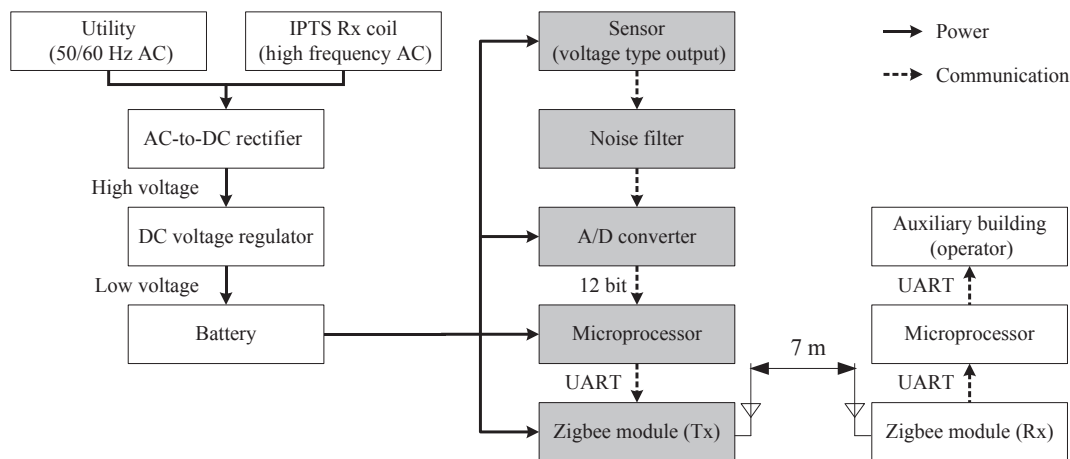

Fig. 6 – Block diagram of the proposed wireless communication channel with a Zigbee-type communication, where a 5-W level wireless sensor set is colored in gray. AC, alternating current; DC, direct current; IPTS, inductive power transfer system; Rx, receiving side; Tx, transmitting side; UART, universal asynchronous receiver/transmitter.
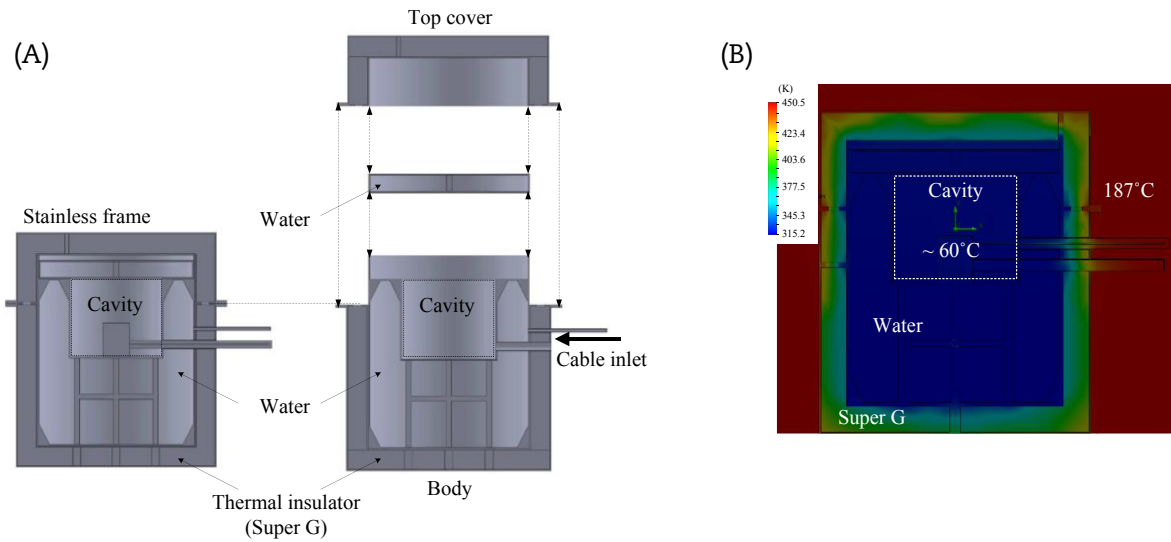
Fig. 7 – Overall configuration and a finite element modelling simulation result of the proposed thermal insulation box. (A) Assembled thermal insulation box (left) and assembly parts (right). (B) Heat transfer simulation result with the temperature profile in Fig. 2 for 72 hours.
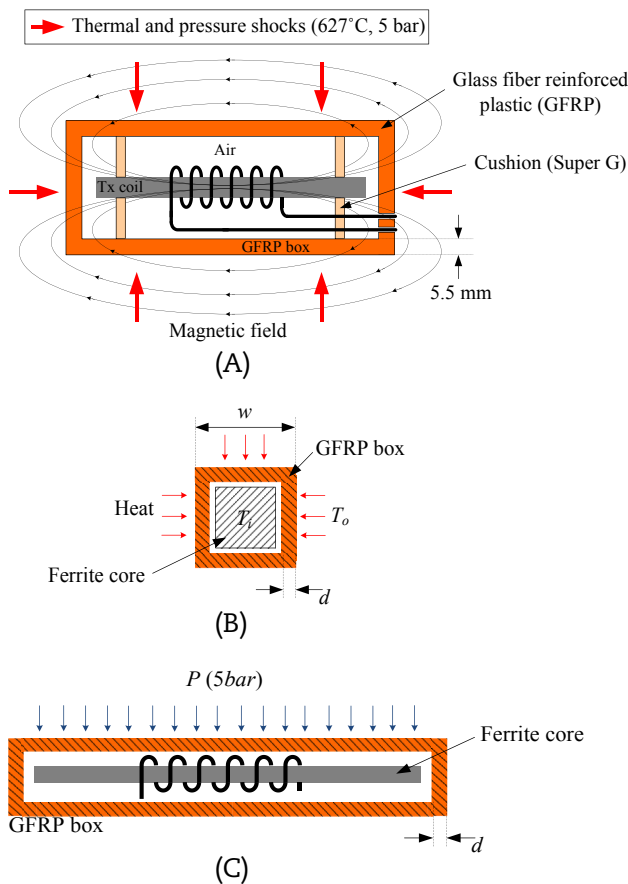

Fig. 8 – The proposed glass-fiber reinforced plastic (GFRP) box for a dipole Tx coil of the proposed wireless power channel. (A) Overall configuration. (B) Side view. (C) Plan view. Tx, transmitting side.

$$k\frac{A}{d}(T_o - T_i) + Q_g = mc\frac{dT_i}{dt} \tag{1}$$

where k, A, d, T_o, T_i, m, c, and Q_g are the thermal conductivity of GFRP, heat conduction cross section area, thickness of GFRP, ambient temperature, dipole coil temperature, mass, specific heat of dipole coil material (ferrite), and heat generation of the dipole coil, respectively.

Considering the external pressure shock, the thickness of the GFRP box can be determined as follows:

$$d > \frac{w}{\sqrt{8\sigma/3P}} \tag{2}$$

Where d, w, P, and σ are GFRP box thickness, GFRP box width, forced pressure on the GFRP box, and ultimate strength of GFRP, respectively.

When the GFRP box is 10-mm thick, the maximum bending stress of 5 bar is lower than the tensile strength of the material. The cavity temperature of the proposed GFRP box slowly increases without any overshoot up to 187°C, which is the long-term ambient temperature under a severe accident. For example, the proposed GFRP box having 10 mm of thickness can delay the cavity temperature increase up to 187°C for 10 hours, where it is assumed that the proposed dipole coil with its power loss of 100 W is located in the cavity.

3.   Experimental verifications

The design results of the proposed highly reliable power and communication system in the previous section are verified with each prototype of four subsystems. To mimic the extreme temperature conditions, a temperature controllable chamber was fabricated to verify the applicability of the thermal insulation box and the GFRP box. Considering the lack of previous studies on the defectiveness of power electronics devices under high radiation, an experimental study was also conducted for

various high-power-applicable circuit components, which are essential to wireless power channels, under a radiative environment having a maximum accumulated dose of 27 Mrad.

3.1.   10-W IPTS over 7-m distance: Performance test with high-temperature and conductive obstacles

The 10-W powering performance of the proposed IPTS was verified, as shown in Fig. 9, where the detail performance
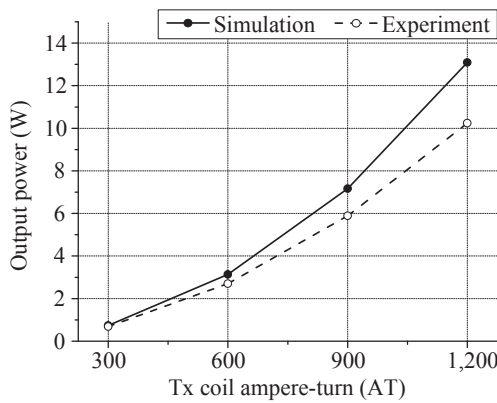

Fig. 9 − Comparison of the simulation results with the experiment results for the proposed inductive power transfer system, where two identical 2-m long dipole coils having 30 turns were used for each transmitting side (Tx) and receiving side coils.

evaluation of a dipole coil resonance system with 2-m long dipole coils over a 7-m distance was conducted in Choi et al. [11]. Changes in several key operating conditions, such as the coil inductance and the compensation capacitances, were experimentally evaluated with respect to high ambient temperature and conductive obstacles between the Tx coil and the Rx coil.

For the high temperature operating test, a quarter scale dipole coil was used with two types of high-frequency applicable polymer film capacitors considering the commercial temperature test chamber TD500, which has a maximum control range from −20°C to 150°C.

Fig. 10 shows variations in the inductance and capacitance of the IPTS according to a temperature sweep ranging from 30°C to 150°C. As identified from Fig. 10A, the inductance variation did not exceed 1.6% of its nominal value, where the IPTS, having a quality factor of 100, allows for an inductance variation of 2%. The series equivalent resistance of the dipole coil was constant during the test, as shown in Fig. 10A.

However, capacitance variations in the two polymer film capacitors, where one is a plastic-cased type and the other one is an epoxy-lacquer-coated type, were more prominent than that of the coil inductance variation. The capacitance of the plastic-cased type increased by 2%, and the capacitance of the epoxy-lacquer-coated type decreased by 1%, as shown in Figs. 10B and 10C, respectively. The capacitance variation can be neglected when both capacitors are used together considering their complementary characteristics against temperature change.

To identify the effect of conductive obstacles on the powering characteristic, the dipole coil inductance was measured,
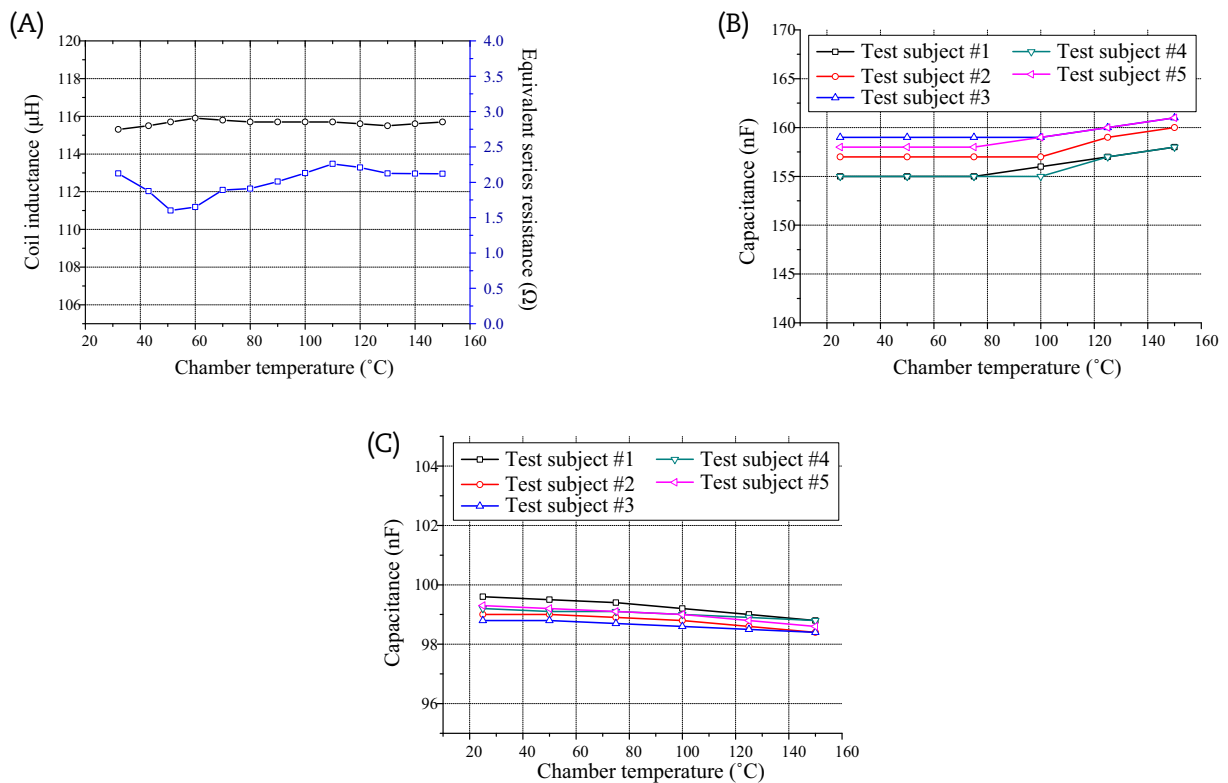

Fig. 10 − High temperature operating test results. (A) Quarter scale dipole coil. (B) Plastic-cased film capacitor. (C) Epoxy-lacquer-coated film capacitor.
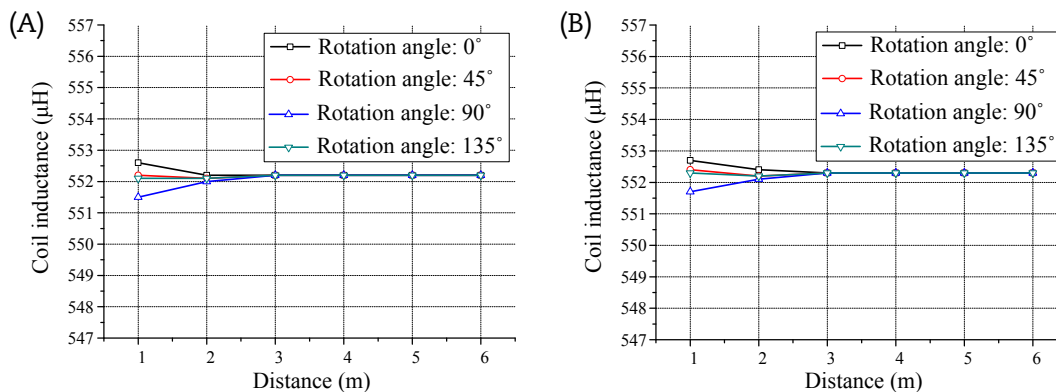
Fig. 11 − Coil inductance variation measurement test with 1-m² sized steel plate according to distance and angles for two different operating frequencies. (A) Maximum variation was 0.2% at 20-kHz operation. (B) Maximum variation was 0.18% at 100-kHz operation.

where a 1-m² sized stainless steel plate was in a different position within a 1−6-m distance range and a 0−135° angle range between the aluminum plate and the coil. As shown in Fig. 11, the coil inductance changed less than 0.2% from its nominal value of each operating frequency case.

From the performance verifications in this section with previous works in Choi et al. [11], it is proven that the IPTS, having a relatively low quality factor of 100, is applicable as the emergency back-up power source under a severe accident environment.

3.2. Zigbee wireless communication: Data loss measurements with conductive surroundings

As shown in Fig. 12, the proposed wireless communication channel was fabricated with a commercial Zigbee module (XB24CZ7PIS-004) and a microprocessor (Dspic30f6012A), where the measured total power consumption of devices above was less than 0.5 W.

For evaluating the applicability of the commercial Zigbee modules during a severe accident, two conductive surroundings were applied during the test. Data losses between the Tx module and the Rx module were measured when one of them
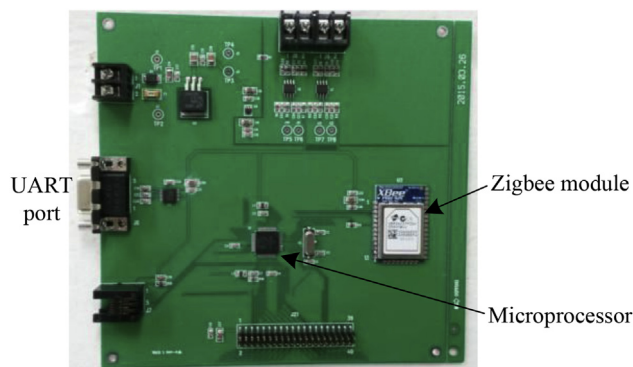
was located inside of a metal box with variable layers, as shown in Fig. 13. Two different metals were used: one was stainless steel and the other was aluminum. There was no data loss in the 7-m distance Zigbee communication with both the stainless steel box and the aluminum box, even though the number of layers increased up to four in both cases.

To mimic ionized spray under hydrogen and steam emissions in the containment building, conductive saline solutions of variable concentrations from 0% to 10% was used, as shown in Fig. 14. Fabric soaked with saline solution, which mimicked the excess of moisture around the Zigbee module, as shown in Fig. 14A, did not cause any data loss during the communication. However, data loss increased as the depth of the saline solution increased, as one of the Zigbee modules sank into the solution, as shown in Figs. 14B and 14C.

3.3. Dynamic temperature test ranging from 627°C to 187°C: Thermal insulation box and GFRP box

A 3.4-m³ sized high temperature test chamber, which was controlled by following the temperature profile in Fig. 1, was fabricated for performance tests of both the thermal insulation box and the GFRP box, as shown in Fig. 15.

The fabricated thermal isolation box, which has a Super G layer and a water layer for a cavity of 0.01 m³, is depicted in Fig. 16A. As shown in Fig. 16B, the Super G layer was intensified with the design margin of 20% in thickness to compensate for a structural defect in the stainless frame, which is mainly
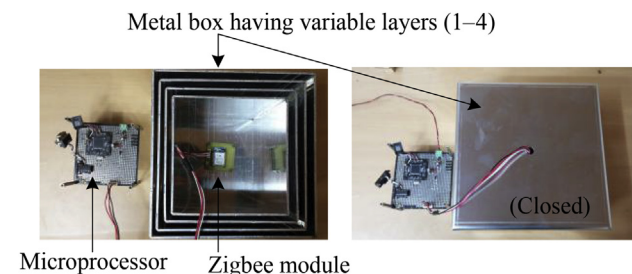

Fig. 12 − Fabricated transmitting module for the proposed wireless communication channel, which is identical to the receiving module. UART, universal asynchronous receiver/transmitter.

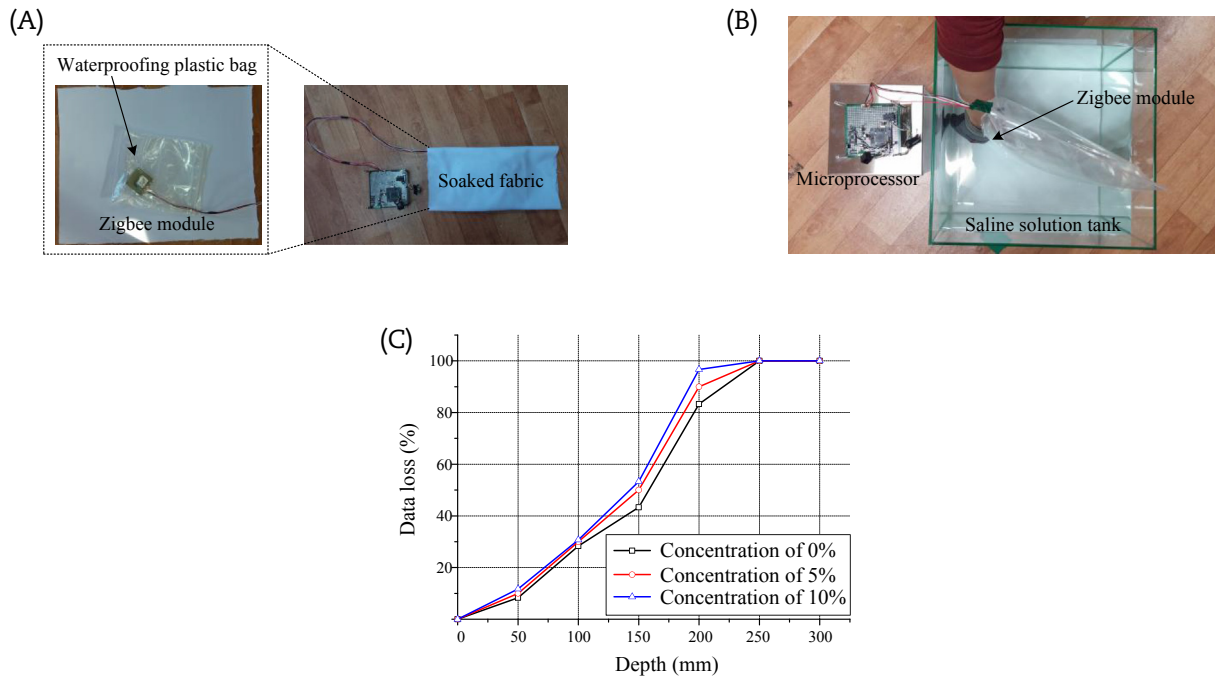**Fig. 13 − Data loss measurement condition with metal boxes.**

Fig. 14 – Data loss measurements with a conductive saline solution. (A) Test condition with soaked fabric. (B) Test condition with a water tank filled with the saline solution. (C) Test results according to different depths and concentrations.

due to imperfect welding conditions. The comparison between the experimental result and the simulation results for 72 hours is shown in Fig. 16B. After the dynamic temperature test, the cavity temperature was 62°C, which is slightly lower than the simulation result due to the design margin of 20% in the thickness of the microporous insulator layer.

A half-scale GFRP box with a 1-m dipole coil was fabricated for the dynamic temperature test due to the limited size of the fabricated test chamber, as shown in Figs. 17A and 17B. The cavity temperature of the fabricated GFRP box reached 187°C 16 hours after initiating the test. Comparing the designed heat transfer delay of 10 hours, a slightly longer delay time was achieved with the help of the Super G cushion, which was mainly used to fix the dipole coil location against vibrations or shocks. Due to the initial heat shock of 627°C, the outer

Fig. 15 – Fabricated dynamic temperature test chamber. GFRP, glass-fiber reinforced plastic.

surface of the GFRP box was partially damaged, as shown in Fig. 17C; however, every important joint part was still robust after the test.

3.4. High radiation test of 27 Mrad: Power electronics device defects

The use of semiconductor-based components is inevitable to build the proposed wireless power and communication channels. Although low power applicable electronic devices have been reviewed under a γ-ray environment for space craft applications [15], most medium-to-high power applicable devices are not tested for their application under a high γ-ray irradiation. In this section, 10 circuit components, which were carefully selected after considering their frequency of use in various power electronics applications, were tested under the high radiation environment for evaluating their application in a severe accident, as tabulated in Table 3. Considering the accumulated dose of a Large Break Loss of Coolant Accident, the devices were tested under the maximum accumulated dose of 27 Mrad at the Korea Atomic Energy Research Institute, where the dose rate of the test environment was 1.2 Mrad/h. Experimental data acquisition was not continuously conducted due to the limited control of the γ-ray experiment environment. However, the experimental results are meaningful as an initial survey to figure out the applicability of power conversion circuits to NPPs.

As shown in Figs. 18A and 18B, there were no considerable changes in capacitance of the film capacitors, where the breakdown voltages were decreased by 32% for the epoxy-lacquer-coated types and 3% for the plastic-cased types after the irradiation. The breakdown voltage was measured with METREL MI 3201, which judges the breakdown when there is a
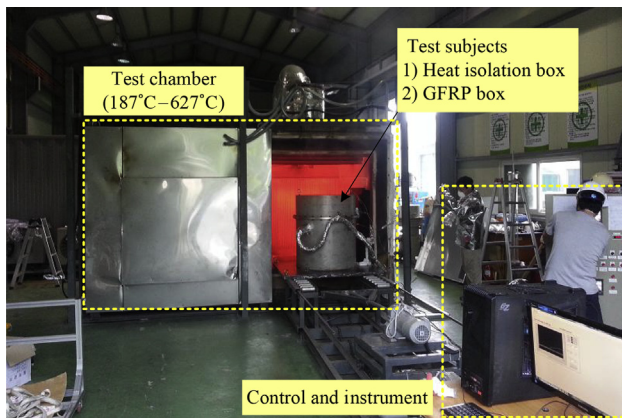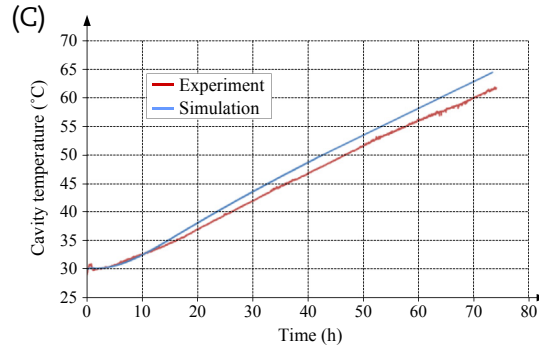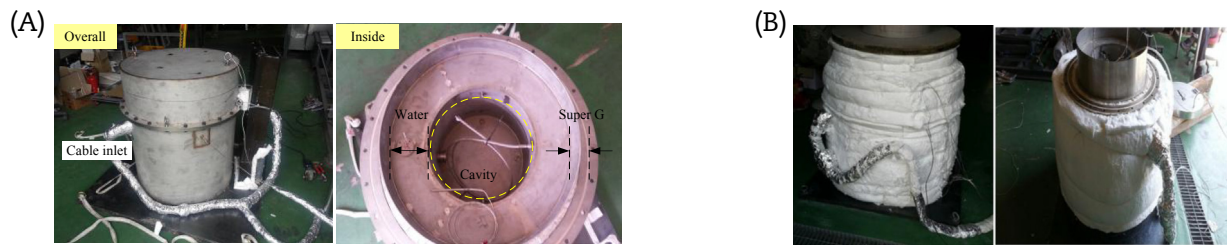
Fig. 16 — Fabricated thermal insulation box and its experimental result for 72 hours. (A) Thermal insulation box. (B) Additional Super G layer around the thermal insulation box. (C) Comparison between the experimental result and the simulation result.
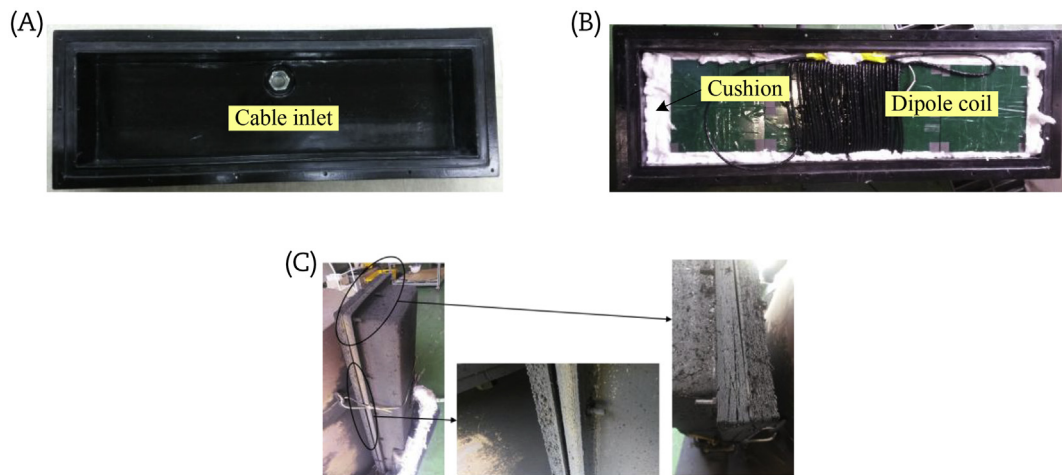

Fig. 17 — Fabricated half scale glass-fiber reinforced plastic box with the dipole coil. (A) Without a dipole coil. (B) With a dipole coil inside. (C) Outer surface condition of the glass-fiber reinforced plastic box after the test.

Table 3 — Summary of the irradiation test.		
Test items	Survivability	Remarks
Film capacitor	O	3–30% decrease in the breakdown voltage
SiC diode	O	2.5% decrease in the breakdown voltage
Zener diode	O	—
Opamp	X	Failure after 0.6 Mrad
SiC JFET	Δ	6% increase in drain-to-source resistance
BJT	O	—
MCU	X	Failure after 20 kRad
IGBT	O	—
SMPS	X	Failure in internal IC devices
Zigbee module	X	Failure in internal IC devices

BJT, bipolar junction transistor; IC, integrated circuit; IGBT, insulated-gate bipolar transistor; JEFT, junction field-effect transistor; MCU, microcontroller; SiC, silicon carbide; SMPS, switched-mode power supply.
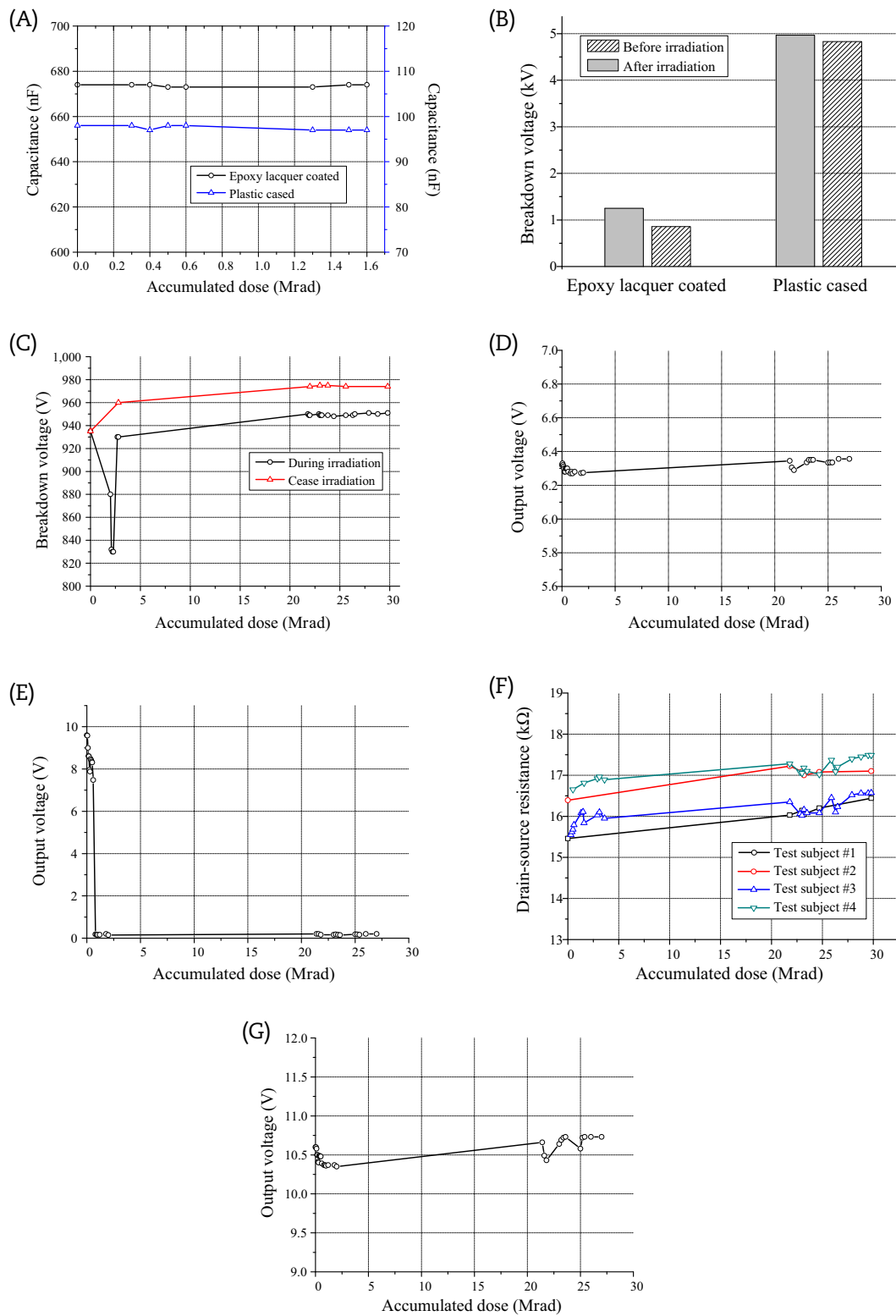
Fig. 18 – **Measurement results of irradiation test for various power electronics devices. (A) Capacitance of two film capacitors. (B) Breakdown voltage change of film capacitors. (C) Breakdown voltage of silicon carbide diode. (D) Output voltage of Zener diode test circuit. (E) Output voltage of Opamp test circuit. (F) Drain-source resistance of silicon carbide junction field effect transistor. (G) Output voltage of bipolar junction transistor test circuit.**
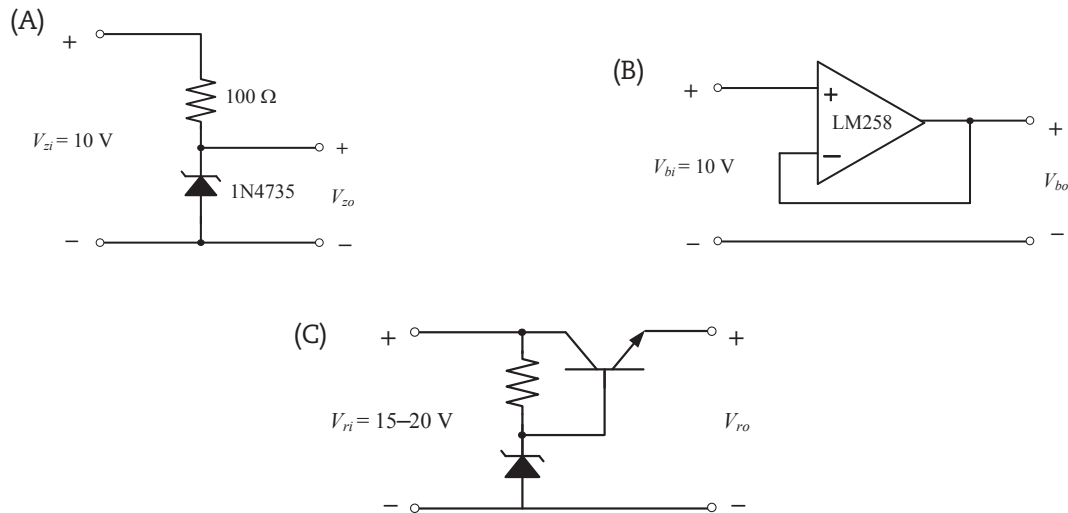
Fig. 19 – Irradiation test circuits. (A) Zener diode. (B) Opamp. (C) Bipolar junction transistor.

leakage current of 1 mA between two test nodes. Considering constant capacitance regarding the accumulated dose, the test on the film capacitors was closed at 1.6 Mrad.

The breakdown voltage of SCS120AG, having its original breakdown voltage of 930 V, which is a silicon carbide diode, was measured, as shown in Fig. 18C. The γ-ray irradiation was intermittently stopped to check recovery characteristics during the radiation test. The breakdown voltage drastically decreased by 21% at the initial irradiation compared to the original value. During interruptions to the irradiation, the breakdown voltage temporally restored a little; however, it decreased again when the irradiation was restarted.

The Zener breakdown voltage was measured with a test circuit including a Zener diode (1N4735A) in Fig. 19A, where the theoretical output voltage V_{zo} was 6.2 V with an input voltage V_{zi} of 10 V. As identified from Fig. 18D, there was no significant defect in Zener breakdown voltage during the test.

The operation of operational amplifiers (op-amps) were tested with a buffer circuit configuration in Fig. 19B. As shown in Fig. 18E, the output voltage V_{bo} of the buffer, which was designed to follow the input voltage V_{bi}, gradually decreased after the initial irradiation; then, V_{bo} dropped to zero when the accumulated dose was 0.6 Mrad.

A slightly increased drain-to-source (DS) resistance of the junction gate field effect transistor was measured, where its gate and source had the same potential, as shown in Fig. 18F. The 6% increased DS resistance indicates higher conduction losses; hence, thermal management systems, such as a heat sink and a fan, should be designed with sufficient margins when they are installed with the junction gate field effect transistor in the high radiation condition. However, the increased DS resistance was decreased to the initial value 2 days after the experiment was terminated.

Using the normal operation of the Zener diodes, a linear regulator circuit was fabricated to evaluate the performance of the bipolar junction transistor, as shown in Fig. 19C. As shown in Fig. 18G, the regulator output voltage V_{ro} was maintained at 10.7 V, which matched well with the theoretical value with the variable input voltage V_{ri} ranging from 15 V to 20 V.

The microprocessor, which was used for prototyping the proposed wireless communication channel, malfunctioned and never restored at the initial stage of the test when the accumulated dose was only 80 kRad.

Due to the difficulties of online experiments, the following components were tested after the irradiation of 27 Mrad: (1) the insulated gate bipolar transistor had no operational defects; (2) a commercial switched mode power supply, which is UHE-15/2000-Q12-C from MURATA Co., Ltd. in this paper, did not survive due to a control circuit failure; (3) a commercial Zigbee module, which was used for the proposed wireless communication, had a permanent defect after the test.

The test results are summarized in Table 3. It is noteworthy that the passive components and the semiconductor devices, having relatively large doping areas, tend to be robust under the high radiation environment, where every integrated-circuit-based device is disabled.

4. Conclusion

A highly reliable power and communication system for the essential equipment in NPPs has been designed with relevant physical reinforcements and has been experimentally verified in this paper. Both the temperature and pressure profiles of the containment building for 72 hours after a severe accident were determined and firstly applied in NPP equipment designs. Wireless power and communication channels were proposed for increasing redundancy in conventionally installed wired channels, where both IPTS and Zigbee communication were adopted under extreme environments. Two major difficulties in the equipment design, high temperature of 627°C and high pressure of 5 bar, were solved by adopting a thermal insulation box and a GFRP box. The performances of prototypes of each subsystem were fully verified with the dynamic temperature test, using a fabricated high-temperature chamber. A γ-ray irradiation test of 30 Mrad was conducted for various power electronics devices to evaluate their use in a high radiation environment, which causes critical defects in most

semiconductor devices. Due to its versatile applicability to currently installed equipment without any interference, the proposed wireless channels and protective boxes can be widely applied to both currently operating NPPs and future NPPs as practical responses to the Fukushima accident.

Conflicts of interest

All authors have no conflicts of interest to declare.

Acknowledgments

REFERENCES

[1] International Atomic Energy Agency, Severe Accident Management Programs for Nuclear Power Plants, IAEA safety standards, No. NS-G-2.15, Austria, 2009.

[2] International Atomic Energy Agency, IAEA International Fact Findings Expert Mission of the Fukushima Daiichi NPP Accident Following the Great East Japan Earthquake and Tsunami, IAEA mission report, Austria, 2011.

[3] Electric Power Research Institute, EPRI Fukushima Daini Independent Review and Walkdown, EPRI 2011 technical report, USA, 2011.

[4] Institute of Nuclear Power Operations, Special Report on the Nuclear Accident at the Fukushima Daiichi Nuclear Power Station, INPO 11−005, USA, 2011.

[5] T. Takeuchi, A. Shibata, H. Nagata, K. Miura, T. Sano, N. Kimura, N. Otsuka, T. Saito, J. Nakamura, K. Tsuchiya, Development of instruments for improved safety measure for LWRs, 5th International Symposium on Material Testing Reactors, Bariloche, Argentina, October 28−31, 2012.

[6] Government of Japan: Nuclear emergency response headquarters, Report of Japanese Government to the IAEA Ministerial Conference on Nuclear Safety, Japan, 2011.

[7] S.J. Yoo, B.H. Choi, S.Y. Jung, C.T. Rim, Highly reliable power and communication system for essential instruments under a severe accident of NPPs, Transactions of the Korean Nuclear Society Autumn Meeting, Gyeongju, Korea, October 23−25, 2013.

[8] S.J. Yoo, B.W. Gu, B.H. Choi, S.I. Lee, C.T. Rim, Development of highly survivable power and communication system for NPP instruments under severe accident, Transactions of the Korean Nuclear Society Autumn Meeting, Pyeongchang, Korea, October 30−31, 2014.

[9] S.I. Lee, H.K, Jung, Development of the NPP instruments for highly survivability under severe accidents, Transactions of the Korea Society for Energy Engineering Autumn Meeting, Jeju, Korea, November 21−22, 2013.

[10] Electric Power Research Institute, Large-scale Hydrogen Burn Equipment Experiments, EPRI NP-4354s, USA, 1985.

[11] S.Y. Jung, B.H. Choi, S.J. Yoo, B.W. Gu, C.T. Rim, A study on the application of wireless power transfer technologies in metal shielding spaces, Transactions of the Korean Institute of Power Electronics Annual Meeting, Gyeongju, Korea, July 2−5, 2013.

[12] B.H. Choi, V.X. Thai, E.S. Lee, J.H. Kim, C.T. Rim, Dipole-coil-based wide-range inductive power transfer systems for wireless sensors, IEEE Trans. Ind. Electron. 63 (2016) 3158−3167.

[13] M. Yoo, S.M. Shin, H.G. Kang, Development of instrument transmitter protecting device against high-temperature condition during severe accidents, Sci. Technol. Nucl. Ins. 2014 (2014) 1−8.

[14] Office of Nuclear Regulatory Research, Regulatory Guide 1.180, US Nuclear regulatory commission, USA, 2003.

[15] M.V. O'Bryan, K.A. LaBel, J.A. Pellish, J.-M. Lauenstein, D. Chen, C.J. Marshall, M.C. Casey, R.A. Gigliuto, A.B. Sanders, T.R. Oldham, H.S. Kim, A.M. Phan, M.D. Berg, P.W. Marshall, R.L. Ladbury, E.P. Wilcox, A.J. Boutte, P.L. Musil, G.A. Overend, Compendium of recent single event effects for candidate spacecraft electronics for NASA, IEEE Nuclear & Space Radiation Effects Conference, San Francisco, CA, July 8−12, 2013.